Tellus (1994), 46A, 242–264
Printed in Belgium – all rights reserved

TELLUS
ISSN 0280–6495

Diabatic initialization for improvement in the tropical analysis of divergence and moisture using satellite radiometric imagery data

By AKIRA KASAHARA* and ARTHUR P. MIZZI, *National Center for Atmospheric Research*[1], *P.O. Box 3000, Boulder, CO 80307, USA*, and LEO J. DONNER, *Geophysical Fluid Dynamics Laboratory/NOAA, Princeton University, Princeton, NJ 08540, USA*

(Manuscript received 2 February 1993; in final form 30 August 1993)

ABSTRACT

To improve the quality of horizontal divergence and moisture analyses in the tropics, a diabatic initialization scheme is developed to incorporate information on convective activity and the proxy data of precipitation obtained from satellite radiometric imagery data. The tropical precipitation rates are estimated by developing a relationship between the pentad precipitation data of the Global Precipitation Climatology Project with *daily* outgoing longwave radiation data. The tropical belt from 35°S to 25°N (for January 1988) is divided into 3 parts: convective, convective fringe, and downward-motion (clear-air) areas. In the convective region, the algorithm adjusts the horizontal divergence and humidity fields such that a version of the Kuo cumulus parameterization will yield the precipitation rates closest to the proxy data. The temperature in the planetary boundary layer is also adjusted, if necessary, to ensure the initiation of cumulus convection. In the downward-motion region, the divergence field is adjusted to yield descending motion expected from the thermodynamic balance between radiative cooling and adiabatic warming. In the convective fringe region, where convective criteria are not met, the divergence field is adjusted only to satisfy the global conservation of divergence. The humidity field is left intact in both the downward-motion and convective fringe regions. This adjustment scheme will ameliorate problems associated with spinup of precipitation in a numerical prediction model with the same cumulus parameterization as used in the initialization. This initialization scheme may be used as a method of quality control for first-guess fields in four-dimensional data assimilation by means of satellite radiometric imagery data.

1. Introduction

Earlier, Kasahara et al. (1988) proposed a scheme, referred to as divergence adjustment (DIVADJ), to improve the analysis of the horizontal divergence by incorporating satellite imagery data into the specification of initial conditions for a global prediction model. It was hoped that the application of this scheme would improve precipitation forecasts in the tropics. However, improvement of divergence analysis alone did not bring about its direct benefit, due to the lack of initialization for the physical processes. This was manifested as the precipitation spinup problem, i.e., prediction model's inability to produce realistic precipitation rates at the beginning of the forecast period.

Recently, significant progress was made in understanding the cause of precipitation spinup problems in tropical forecasts (Illari, 1987; Krishnamurti et al., 1988; Donner and Rasch, 1989; Kasahara et al., 1992). Conventional diabatic initialization suppresses gravity-wave noise, but it cannot ameliorate the spinup problem because: (1) the diabatic information is usually inadequate

* Corresponding author.

[1] The National Center for Atmospheric Research is sponsored by the National Science Foundation.

for tropical initialization, (2) there is no initialization of the moisture field, and (3) no specific consideration is made to ensure that the initiation of cumulus convection reflects reality. We found that the adjustments of moisture and temperature (TNQADJ), using the cumulus initialization developed by Donner (1988), are essential to ameliorate the spinup problem.

The standard practice of initialization is to apply the diabatic nonlinear normal mode initialization (NNMI) to the analyzed data for suppression of the dynamic imbalance, using diabatic heating information obtained by short-time integrations with the prediction model. A better estimate of the heating rate can be obtained by using proxy satellite data to adjust the model-generated heating, producing beneficial impacts on tropical forecasts (Puri and Miller, 1990; Heckley et al., 1990). Our experience, however, shows that the improvement of diabatic heating information in diabatic NNMI alone does not ameliorate the spinup problem and the operations DIVADJ and TNQADJ make significant impacts on improvement in the precipitation spinup characteristics. Because the application of both DIVADJ and TNQADJ can upset dynamical balance, reapplication of diabatic NNMI is useful, though possibly necessitating another application of TNQADJ. See Kasahara et al. (1992) for the impact of various initialization components upon the spinup of precipitation forecasts and Fig. 4 in the same article for a schematic diagram of various steps of initialization.

The objective of this study is to develop a unified approach to diabatic initialization, combining the separate steps of DIVADJ and TNQADJ through incorporation of satellite radiometric imagery data, which provide proxy data for the precipitation rate.

2. Rationale for the present research

The current four-dimensional meteorological data assimilation schemes employed at forecasting centers are primarily designed to analyze the mass (pressure and temperature) and rotational wind field accurately in the middle to higher latitudes (Daley, 1991). In fact, even the adiabatic NNMI is effective in diagnosing the vertical motion field in the middle to higher latitudes, due to strong baroclinicity coupled with rotational and thermal stability (a large Richardson number). Except for the Southern Hemisphere, where conventional observations are relatively deficient, the current data assimilation systems are satisfactory in the middle to higher latitudes, even for vertical motion and moisture analyses. (Clearly this circumstance does not apply to mesoscale systems, but consideration of mesoscale analysis is beyond the present scope.)

Now, the situation of tropical analysis is quite different from the middle to higher latitude analysis. It is well known that the analyses of horizontal divergence and moisture are unreliable in the tropics, as reflected by large disagreement in their daily values analyzed at operational centers (Trenberth and Olson, 1988; Lambert, 1989; Mizzi and Kasahara, 1989; and Kasahara and Mizzi, 1992). The multivariate optimal (statistical) interpolation (OI) analysis schemes that have been used by many operational centers are essentially designed to analyze the rotational part of the wind. They are relatively ineffective in the tropics due to the lack of simple dynamical relationships between mass and wind field, and the magnitude of the divergent wind component is generally the same order of magnitude as the errors in wind measurements (Hollingsworth et al., 1989). The vast majority of wind observations over the tropics are at a single level, most of which are provided through satellite cloud tracking. While these wind data are undoubtedly useful, they provide little information on the vertical structure needed for multi-level synoptic analysis. In addition, the moisture field analysis is ordinarily performed univariately and heavily relies on the first-guess field because of the shortage in the number of radiosonde water vapor observations (Pasch and Illari, 1985), unless they are supplemented by bogus moisture data with the use of satellite cloud data (e.g., Baba, 1987; Mills and Davidson, 1987). Because the water vapor field is tied closely to the horizontal divergence field, the quality of the water vapor first-guess field is likely similar to that of the horizontal divergence first-guess field. Therefore, even though the divergence effect can be included in the OI schemes (Undén, 1989), the analysis of irrotational wind and moisture in the tropics is problematic.

The approach described here is intended to be a tropical initialization scheme for cumulus convection, but it can be looked upon as an adjustment

scheme applicable to the first-guess fields of temperature, divergence (or irrotational wind), and moisture as a means of quality control. The current analysis procedures generally adopt six-hour forecasts as first-guess fields for the analysis cycle without checking the quality of the forecasts. Recently, Puri and Davidson (1992) and Mathur et al. (1992) are developing initialization schemes for moisture with the aid of satellite-derived proxy data of rainfall that are applicable to the first-guess moisture field for correction in the data assimilation systems. The forecast quality of the vorticity (or rotational wind) field may be difficult to check. This may also be true in the case of temperature forecasts to a large extent, but at least over convective regions the quality of temperature forecasts can be examined. Along a similar line, if we assume that satellite radiometric imagery data in the tropics can identify the areas of ascending and descending motions to the scales of cloud clusters, the quality of vertical velocity fields in the tropics can be checked, as we discuss later. Although one sensitive issue relates to the identification of non-precipitating cirrus clouds, the identification of deep cumulus convection areas should be relatively straightforward.

First, let us discuss the determination of vertical velocity in cloud-free areas in the tropics. As shown in the *Appendix*, the large-scale vertical velocity in the tropics can be estimated with reasonable accuracy, if the large-scale distribution of diabatic heating is known. In other words, adiabatic warming due to descending motion in cloud-free areas should primarily be balanced by radiative cooling. One problem to investigate is the sensitivity of the radiative cooling to uncertainties in moisture analysis. Nevertheless, a gross check in the magnitude of downward velocity can be performed diagnostically using the balance requirement discussed in the *Appendix*.

Second, we consider how to check the vertical velocity and water vapor in deep convection areas of the tropics. Again, we can invoke the approximation that vertical velocity is estimated from the distribution of diabatic heating. The problem is that, in convective areas, the principal component of diabatic heating is the latent heat of condensation, released by convection. This heating rate, unlike radiative cooling rates in cloud-free areas, is difficult to obtain from the prediction model unless the forecast of convective areas happens to be correct. Clearly, we need observed condensation heating data to estimate the analysis quality of vertical velocity. However, it is difficult to obtain the vertical distribution of latent heating from observations, while the vertically integrated total convective heating (or precipitation rate) in the air column may be observable. We assume, then, that such proxy data, possibly including the vertically integrated total precipitable water in the air column, are provided by remote sensing observations, such as measurements from the Special Sensor Microwave/Imager (SSM/I) (Spencer et al., 1989) and the Satellite Tropical Rainfall Mission (TRMM) (Theon and Fugono, 1988). Because these observed data are vertically integrated quantities, we must develop a technique to partition them vertically. We must also investigate the use of these data for determining the vertical distributions of moisture and horizontal divergence together, since these two variables are physically coupled in moist convection through the cumulus parameterization in a prediction model.

If the vertical distributions of moisture, temperature, and horizontal divergence of the analyses were ideal, the vertically integrated precipitation and precipitable water in the air column would agree with the proxy data. In reality, we must expect some discrepancies to occur. For example, if the air temperature near the surface is too low and it is undersaturated, cumulus convection will not occur. If the proxy data show that there should be deep convection and the surface fluxes of moisture and sensible heat are known, the moisture and temperature near the earth's surface should be adjusted to ensure the initiation of convection. Of course, if the vertical distributions of divergence, moisture, and temperature were inappropriate, then we cannot hope that the cumulus parameterization will produce the expected amount of rainfall. How to adjust the vertical distributions of temperature, divergence, and moisture in the tropics using the information of precipitation rate is discussed in the following sections.

3. Adjustment of temperature, horizontal divergence, and moisture in the convective area

To be specific in describing the adjustment algorithms, we adopt a version of the NCAR Com-

munity Climate Model-1 (CCM1), described by Williamson et al. (1987), as our atmospheric model. The CCM1 is a primitive equation model with spherical harmonics triangular-42 truncation in the horizontal with a Gaussian grid of 128 longitudes and 64 latitudes and 12 unequally spaced sigma levels in the vertical (see Table 1). This version of the CCM1 adopts the Kuo (1974) cumulus parameterization, which is subjected to large-scale moisture convergence and conditional instability, coupled with a one-dimensional, buoyancy-driven cumulus cloud model. This cloud model consists of the steady-state equations for cloud vertical momentum and temperature of an ascending air parcel (Donner et al., 1982).

3.1. Temperature T

In the temperature adjustment of Donner (1988), it was assumed that an approximate form of the vertical distribution of convective heating rate is known. Also, the adjustment scheme applies to the entire air column. Since the vertical distribution of temperature in the tropical free atmosphere is ordinarily conditionally unstable, Donner's original temperature adjustment scheme may be simplified by modifying the temperature in the lower troposphere only.

Let subscript h refer to the height of the planetary boundary layer, which is assumed to coincide with the lowest sigma level of CCM1, $\sigma = 0.991$. Here, $\sigma = p/p_s$ with p being the pressure and p_s the surface pressure. We assume here that the boundary-layer temperature T_h and boundary-layer specific humidity q_h are given. Alternatively, if the surface fluxes of heat, momentum, and moisture at $\sigma = 1$ are known, T_h and q_h will be calculated using the inversion of CCM1 flux parameterizations, provided that the surface temperature T_s is also known. Krishnamurti et al. (1991) developed an inversion scheme to obtain the potential temperature and the moisture variable on top of the constant flux boundary layer from given fluxes of sensible heat and latent heat.

Table 1. *Vertical coordinates of the NCAR CCM1*

Index k	σ level	$\Delta\sigma_k$
	0.009	0.0170
2	0.025	0.0255
3	0.060	0.0425
4	0.110	0.0525
5	0.165	0.0675
6	0.245	0.0950
7	0.355	0.1275
8	0.500	0.1545
9	0.664	0.1555
10	0.811	0.1310
11	0.926	0.0900
12	0.991	0.0415

Now, the pressure of the lifting condensation level p_{LCL} is obtained as the level of saturation when an air parcel with its temperature T_h and moisture content q_h is lifted adiabatically. Since the saturation specific humidity q_{sat} is represented as a function of T and p, the pressure p_{LCL} is calculated from a transcendental equation in the following form:

$$q_h = q_{sat}[T_h(p_{LCL}/p_h)^{\kappa}],$$

where κ denotes R_d/C_p, the ratio of gas constant for dry air over the specific heat of dry air at constant pressure.

In the convective region, an air parcel may continue to ascend beyond p_{LCL} following the cloud saturation adiabat dT_c/dp and reach the pressure level of free convection p_{LFC}. The cloud temperature T_c at p_{LFC} is, therefore, determined by

$$T_c(p_{LFC}) = T_h\left(\frac{p_{LCL}}{p_h}\right) \int_{p_{LCL}}^{p_{LFC}} \left(\frac{dT_c}{dp}\right) dp, \tag{3.2}$$

where

$$\frac{dT_c}{dp} = \left[\left(1 + \frac{Lq_c}{T_{cv}R_d}\right)\frac{}{\rho C_p}\right] \times \left[1 + \frac{R_d L^2 e_{sat}}{pC_p R_v^2 T_c^2}\right] \tag{3.3}$$

where T_{cv} denotes the cloud virtual temperature, L the latent heat of condensation, q_c the cloud specific humidity, e_{sat} the saturation vapor pressure at T_c, R_v the gas constant for water vapor, and ρ the density of air.

To ensure the occurrence of free convection, the environmental (large-scale) temperature T must be less than T_c right above the level of p_{LFC}. If this is not the case in the convective region, the large-

scale temperature directly above p_{LFC} should be modified to ensure convection at the LFC. According to results obtained by Thompson et al. (1979) with respect to undiluted air parcels displaced upward from 1000 hPa over the GATE area in the Atlantic, p_{LCL} and p_{LFC} are 964 hPa and 922 hPa, respectively, in the trough category. We, therefore, assume that p_{LFC} is less than p_{LCL} by 42 hPa in the convective region. We then propose adjusting the two model-level temperatures, T_{km} and T_k at p_{km}/p_s and p_k/p_s directly above and below the level of p_{LFC}/p_s (see Fig. 1) to ensure convection. Let ΔT_{km} and ΔT_k be the adjustments to T at levels km and k, respectively. These values are determined to satisfy the following condition for free convection

$$T(p_{LFC}/p_s) = a(T_k + \Delta T_k) + b(T_{km} + \Delta T_{km}) \leqslant T_c(p_{LFC}/p_s), \tag{3.4}$$

where

$$a = (p_{LFC} - p_{km})/(p_k - p_{km})$$

$$b = (p_k - p_{LFC})/(p_k - p_{km}),$$

with the constraint that the temperature variance, $(\Delta T_k)^2 + (\Delta T_{km})^2$, be minimized. The optimum values of ΔT are found by solving a linearly constrained quadratic programming problem.

3.2. *Specific humidity q and horizontal divergence D*

This is an extension of the humidity adjustment scheme (Donner, 1988) to include the basic idea of DIVADJ (Kasahara et al., 1988).

The convective heating Q_c in units of K s^{-1} in the ascending motion area as given by Donner (1988) is

$$Q_c = \frac{L(1-b)\, gM(T_c - T)}{C_p \int_{p_t}^{p_b} (T_c - T)\, dp} \tag{3.5}$$

where

$$gM = -\int_0^{p_s} V \cdot \nabla q + qD)\, dp + gM_s, \tag{3.6}$$

$$(1-b) = \frac{1}{0.7p_s} \int_{0.3p_s}^{p_s} (q/q_{sat})\, dp. \tag{3.7}$$

Here, T, V, q, and D refer to the large-scale temperature, horizontal velocity, specific humidity, and horizontal divergence, respectively; gM is the sum of the large-scale moisture convergence and surface evaporation, denoted by gM_s. The latter quantity is calculated using the formula for surface evaporation (2.f.22) from Williamson et al. (1987). The subscript s refers to the earth's surface. The factor $(1-b)$ denotes the fraction of the large-scale convergence that precipitates. The cloud temperature T_c is calculated by integrating (3.3) with respect to p starting from T_c at p_{LCL}. In (3.5), p_b denotes the cloud base pressure equal to p_{LCL}. Also, p_t denotes the cloud top pressure calculated as the first intersection of T_c with the environmental temperature T moving upward through the column starting at cloud base. We calculate the column-averaged convective heating by integrating (3.5) with respect to p from p_t to p_b,

$$I = (p_b - p_t)^{-1} \int Q_c\, dp = (L/C_p)(1-b)(p_b - p_t)^{-1}\, gM. \tag{3.8}$$

Our task is to find the adjustments to the divergence δD and specific humidity δq with respect to their input values D_i and q_i, such that the substitution of

$$D = D_i + \delta D, \tag{3.9a}$$

and

$$q = q_i + \delta q \tag{3.9b}$$

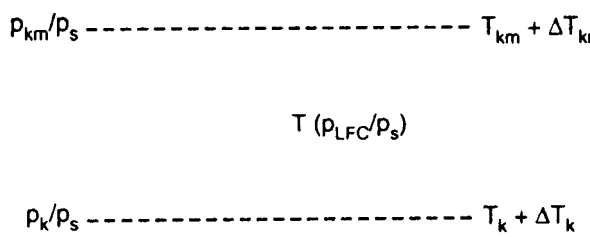

Fig. 1. Adjustment of environmental temperature at model levels p_{km}/p_s and p_k/p_s to ensure that T is less than T_c at p_{LFC}/p_s.

into (3.8) provides an integral I that is close to the observed value I_0. Thus, we should have

$$I_0 = \frac{L}{(p_b - p_t)\, C_p} [(1-b)_i\, gM_i + \delta(1-b)\, gM_i + (1-b)_i\, g\,\delta N + F], \tag{3.10}$$

where the subscript i refers to the input value and δ refers to adjustment. Specifically,

$$(1-b)_i = \frac{1}{0.7 p_s} \int_{0.3 p_s}^{p_s} (q_i/q_{sat})\, dp, \tag{3.11}$$

$$\delta(1-b) = \frac{1}{0.7 p_s} \int_{0.3 p_s}^{p_s} (\delta q/q_{sat})\, dp, \tag{3.12}$$

$$gM_i = -\int_0^{p_s} V\cdot\nabla q + q_i D_i)\, dp + gM_s, \tag{3.13}$$

$$g\,\delta N = -\int_0^{p_s} (\delta q\, D_i + q_i\, \delta D)\, dp, \tag{3.14}$$

$$F = \delta(1-b)\, g\,\delta N - [(1-b)_i + \delta(1-b)] \times \int_0^{p_s} \delta q\, \delta D\, dp. \tag{3.15}$$

Here, we assume that the horizontal moisture advection $V\cdot\nabla q$ and the evaporation gM_s are unchanged by the adjustment.

Solutions δD and δq that satisfy (3.10) within a given tolerance are sought by imposing the following constraints:

(1) The initial surface pressure tendency should not be affected by the adjustment of horizontal divergence. The surface pressure tendency equation is given by

$$\frac{\partial p_s}{\partial t} = -\int_0^1 (D_i + \delta D + V\cdot\nabla \ln p_s)\, d\sigma, \tag{3.16}$$

where $\sigma = p/p_s$. Since we assume that $V\cdot\nabla \ln p_s$ is unchanged by the adjustment, we obtain the following mass conservation condition from (3.16):

$$\int_0^{p_s} \delta D\, dp = 0. \tag{3.17}$$

Constraint (3.17) ensures that the generation of barotropic meteorological noise is suppressed initially consistent with the Machenhauer balance condition (Daley, 1991).

(2) The specific humidity q_h at the lowest model level of CCM1 is unchanged so that $\delta q_h = 0$ at $\sigma = 0.991$. If the surface flux of moisture was known, an improved value of q_h that is obtained from the inversion of CCM1 flux could be used.

(3) The precipitable water P_ω is specified, a priori, so that

$$\int_{0.3 p_s}^{p_s} (q_i + \delta q)\, dp = P_\omega. \tag{3.18}$$

However, this condition is optional, as in the case of moisture adjustment by Donner (1988), and it is not used in this study.

(4) The adjusted relative humidity cannot exceed 95%, so that

$$0.95 q_{sat} \geq q_i + \delta q \geq 0 \tag{3.19}$$

throughout an air column.

(5) The vertical p-velocity $\omega (\equiv dp/dt)$ satisfies the diabatic balance condition (A.16) to a first approximation as discussed in the Appendix. This constraint controls the temporal development of the horizontal divergence. More specifically,

$$p_s^{-1}\omega = -\Gamma^{-1}(Q_R + Q_c), \tag{3.20}$$

where Γ denotes the static stability defined by

$$\Gamma = \frac{R_d T}{C_p \sigma} - \frac{\partial T}{\partial \sigma}, \tag{3.21}$$

which should be positive. Also, Q_R denotes the radiative heating rate, including both shortwave and infrared radiation. The quantity Q_c is the convective heating rate as given in (3.5), but it is expressed in the form

$$Q_c = \frac{\left[L[(1-b)_i\, gM_i + \delta(1-b)\, gM_i + (1-b_i)\, g\,\delta N + F] \right]}{C_p \int_{p_t}^{p_b} (T_c - T)\, dp} \tag{3.22}$$

that follows from the substitution of (3.9) and use of (3.11)–(3.15).

On the other hand, the continuity equation gives the following expression for ω

$$p_s^{-1}\omega = \sigma V\cdot\nabla \ln p_s - \int_0^\sigma (D_i + \delta D + V\cdot\nabla \ln p_s)\, d\sigma. \tag{3.23}$$

Thus, by eliminating $p_s^{-1}\omega$ between (3.20) and (3.23) and using the definition of Q_c by (3.22), we obtain a complicated nonlinear thermal balance constraint involving both δq and δD. Above the cloud top where Q_c vanishes, this balance constraint takes a much simpler form because the relationship between δq and δD as expressed in (3.22) is no longer needed. The descending velocity ω is calculated from (3.20) to maintain thermodynamic balance with radiative cooling, and δD is determined from (3.23).

(6) Adjustments of δq and δD are minimized in the least squares sense, i.e.,

$$\int_0^{p_s} [W_q(\delta q)^2 + W_D(\delta D)^2]\, dp \tag{3.24}$$

is minimized. In (3.24) W_q and W_D denote the weights for the variance of δq and δD, respectively.

Solutions of δq and δD that minimize the integral (3.24) together with the constraints (1) to (5) are obtained by a nonlinearly constrained minimization routine.

As it is discussed in Subsection 6.2, not all points identified as convectively active undergo the adjustment of temperature, divergence, and moisture. Some of the grid points within the precipitating area do not meet the convective criteria, discussed in Subsection 6.2. These are called convective fringe points. We do not modify the input values of horizontal divergence D and moisture for the convective fringe points, except for a minor adjustment of D to satisfy the global conservation of D as discussed in Section 5.

For the implementation of this adjustment scheme as discussed in Section 6, we have chosen the weights W_q and W_D to be unity after normalizing δq by the local saturation specific humidity and δD by the scaling of $5 \times 10^{-6}\ s^{-1}$. The results of the optimization are not sensitive to changes in W_q and W_D, provided they are of order unity, due to imposition of the dynamical constraint (3.20).

4. Determination of δD in descending motion area

Since the horizontal gradient of p_s and the local time rate of change in p_s are both generally very small in the tropics, the vertical p-velocity ω can be approximated by $p_s\dot{\sigma}$. Also, the local time change of T in the tropics is very small. (The effect of diurnal variation in T can be included, if necessary.) Therefore, from the thermodynamic equation we obtain a diagnostic equation for ω of the form

$$\omega = \frac{p_s}{\Gamma}(-Q_R + V\cdot\nabla T), \tag{4.}$$

where Γ is defined by (3.21) and the radiative heating Q_R is calculated using the CCM1 radiation code.

Once ω is obtained, the adjustment δD can be calculated from (3.23). In the descending motion area, no change is made to the temperature and moisture fields, unless the information about the precipitable water is provided. It is straightforward to design an adjustment scheme for moisture if such information becomes available. It should be noted that Krishnamurti et al. (1984) applied the advective-radiative balance to adjust the moisture field in a rain-free area by assuming the horizontal divergence field to be unchanged, while our procedure adjusts the horizontal divergence field by assuming the moisture field to be unchanged. In both cases, the advective-radiative balance is invoked to maintain in the rain-free area. The question of which variable should be adjusted depends upon the circumstance in which the analysis quality of a particular state variable is deemed more deficient than the other in that domain.

The adjustment schemes presented in Sections 3 and 4 are applied to the temperature, divergence, and specific humidity in the tropical belt. The rotational wind field remains unchanged.

5. Remaining adjustment steps

We must ensure that the new divergence field is well blended with the divergence field outside the tropical belt. At the first two rows inside the southern and northern boundaries of the tropical belt, the new D values are weighted by $\frac{1}{3}$ and $\frac{2}{3}$, respectively, to the input D values. This gives a smooth transition from the D values outside the tropical belt to the new D values inside.

Since the divergence field outside the tropics remains unchanged, the area integral of D at each level within the tropical belt should not be changed

to make the global area integral of D vanish. We apply corrections to the adjusted D values by an amount proportional to the magnitude of adjusted D values. Let D_i denote the input divergence and D_a the adjusted divergence. Then the corrected values D_c are calculated from

$$D_c = D_a - C_h |D_a| \tag{5.}$$

where the coefficient C_h is obtained from

$$C_h = \frac{\int_S (D_a - D_i) \cos\phi \, d\phi \, d\lambda}{\int_S |D_a| \cos\phi \, d\phi \, d\lambda} \tag{5.2}$$

and S denotes the area of the tropical belt.

This correction procedure may change the vertical integral of D_c. Thus, we apply a final correction to D_c so that the vertical integral of the final value of divergence D_f vanishes. Hence, we apply the following correction

$$D_f = D_c - C_v |D_c|, \tag{5.3}$$

where

$$C_v = \frac{\int_0^1 D_c \, d\sigma}{\int_0^1 |D_c| \, d\sigma}.$$

This final correction may change the horizontal integral of D_f over the area S, but this difference is too small to necessitate repetition of (5.1).

Once the final divergence field D_f is obtained, the divergent wind component is calculated using the velocity potential χ by solving $D_f = \nabla^2\chi$. The rotational wind component of the input wind field remains unchanged, so that the adjusted wind field is the sum of the input rotational wind and the adjusted divergent wind. The adjusted ω field can be obtained from (3.23) using the final divergence field D_f in place of $D_i + \delta D$.

6. A case study

6.1. *Estimate of precipitation rate*

In this study we assume that the observed column-averaged convective heating I_0, as given by (3.10), is obtained from the precipitation rate. Since daily analyses of tropical precipitation rates are not routinely available, we must construct proxy data for the daily tropical precipitation.

The Global Precipitation Climatology Project (GPCP) has been compiling five-day and monthly precipitation estimates since January 1986 for 40°S–40°N (Janowiak and Arkin, 1991). These data are based on infrared data from geostationary and polar-orbiting satellites using an algorithm developed by Arkin and Meisner (1987). Data on 2.5° latitude-longitude grids are archived at the National Center for Atmospheric Research by the Data Support Section. Since daily outgoing longwave radiation (OLR) data from NOAA-9 are also available for the same period, we estimate a daily precipitation distribution in the tropics by means of a regression relationship between the pentad GPCP precipitation and OLR data. To obtain precipitation data at the standard map time of 1200 UTC, the daytime and nighttime OLR measurements are linearly weighted according to the time of equator crossing using an algorithm described by Julian (1984). Details of the proxy precipitation rate calculation will be described elsewhere. Fig. 2 shows the precipitation rate in the tropical belt, ranging from 35°S to 25°N, for 1200 UTC 1 January 1988. The precipitation rate of 1 cm day^{-1} is converted to a column-averaged convective heating rate of 2.4 K day^{-1}. It turns out that convective heating obtained from the precipitation data has heating maximums of 20 K day^{-1}, which are thought to be too large for synoptic-scale heating. After considerable experimentation we reduced the OLR-based heating rates with the formula $0.8(a - bI_o)\, I_o$, where $a = 1.1$, $b = 0.03$, and I_o is in units of K day^{-1}. The reasons behind this correction are explained in Section 7.

6.2. *Classification of tropical grid points*

We treat grid points with nonzero proxy precipitation rates as convective points eligible for the adjustment of temperature, horizontal divergence, and specific humidity. However, we exclude points that do not meet the criteria for cumulus convection. First, we calculate the cloud temperature profile T_c by integrating (3.3) upward with respect to p from the cloud base p_b indicated by p_{LCL}. The cloud top p_t is positioned as the first point where T_c reaches equilibrium ($T_c = T$). The atmosphere should be convectively unstable to be qualified as a convective point, though we permit a slight degree of stability of less than 1 K between

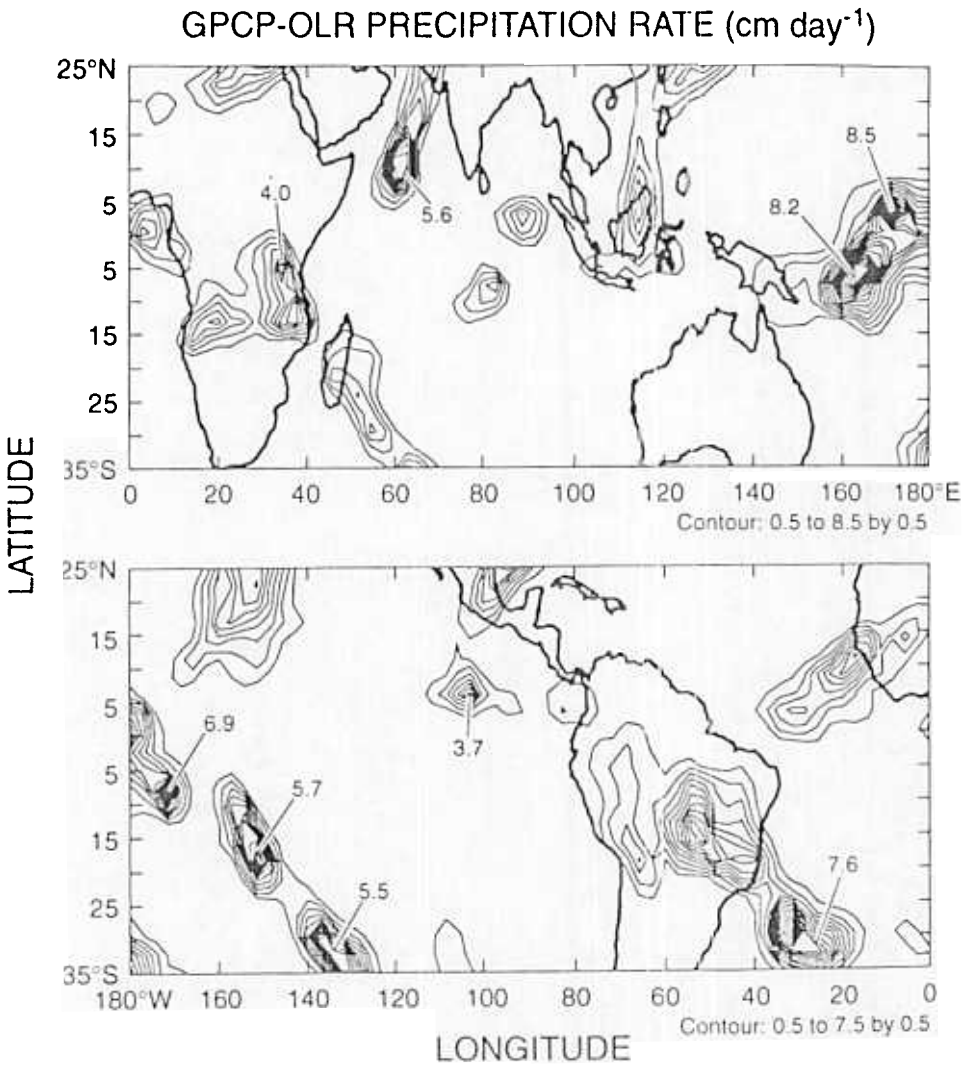

Fig. 2. Geographical distribution of precipitation rate in the tropics in cm day for 1200 UTC January 1988. Contour interval is 0.5 cm day $^{-1}$.

T and T_c at one sigma-level only between p_b and p_t.

We impose the following additional constraints on the convective points and their adjustments.

(1) The magnitude of temperature adjustment described in Subsection 3.1 cannot exceed 3 K.

(2) The cloud base pressure p_b cannot be less than 0.811 times the surface pressure p_s to avoid the points over high topography.

(3) The cloud top pressure p_t cannot be greater than 0.335 times p_s to avoid shallow convective layers.

The descending motion area is defined by the region where the OLR emission temperature T_e is greater than 260 K, which is slightly larger than the value 258 K found by Kasahara et al. (1987). The use of a larger threshold temperature enables us to make a conservative estimate of the number of grid points for the descending motion area. Finally, those grid points that do not belong to either convective area or descending motion area are referred to as the convective fringe points.

6.3. Input data

We apply this diabatic initialization scheme to the input data for 1200 UTC 1 January 1988, from the analysis dataset of the European Centre for Medium-Range Weather Forecasts (ECMWF). The data we use are the horizontal velocity V and geopotential height at 14 pressure levels, the relative humidity below the level of 300 hPa, and

the surface geopotential. These data are interpolated onto the standard CCM1 T-42 grid using the algorithm of Mayer (1988).

6.4. Geographical distribution of vertical p-velocity

The vertical p-velocity ω is calculated from (3.23) using the horizontal velocity V, the horizontal divergence $D = \nabla \cdot V$, and the surface pressure p_s using the CCM1 algorithm. Fig. 3 shows ω from the ECMWF (T-42) analysis at $\sigma = 0.355$ for 1200 UTC 1 January 1988. Comparison of this with the precipitation distribution in Fig. 2 shows some correspondence between precipitation and the upward-motion (negative ω) areas, but we also see upward motion in the areas of no precipitation and downward motion in the areas of precipitation. Since the upward and downward motion have a cellular structure, it is difficult to visualize the organization of a synoptic pattern. In fact, the point of showing Fig. 3 is to remind the reader that useful information contained in the raw analysis field of vertical velocity is difficult to extract, even though the vertical velocity field is considered to be most important in characterizing the tropical circulations. However, we will show later that Fig. 3 does contain a great deal of reality and how to recognize such useful information. Note that the contour interval is 0.1 Pa s^{-1} (86.4 hPa day^{-1}), which corresponds to roughly 10 cm s^{-1}. Clearly, the magnitudes of ascending velocity in some areas are very large.

Now, Fig. 4 shows the adjusted ω at the same

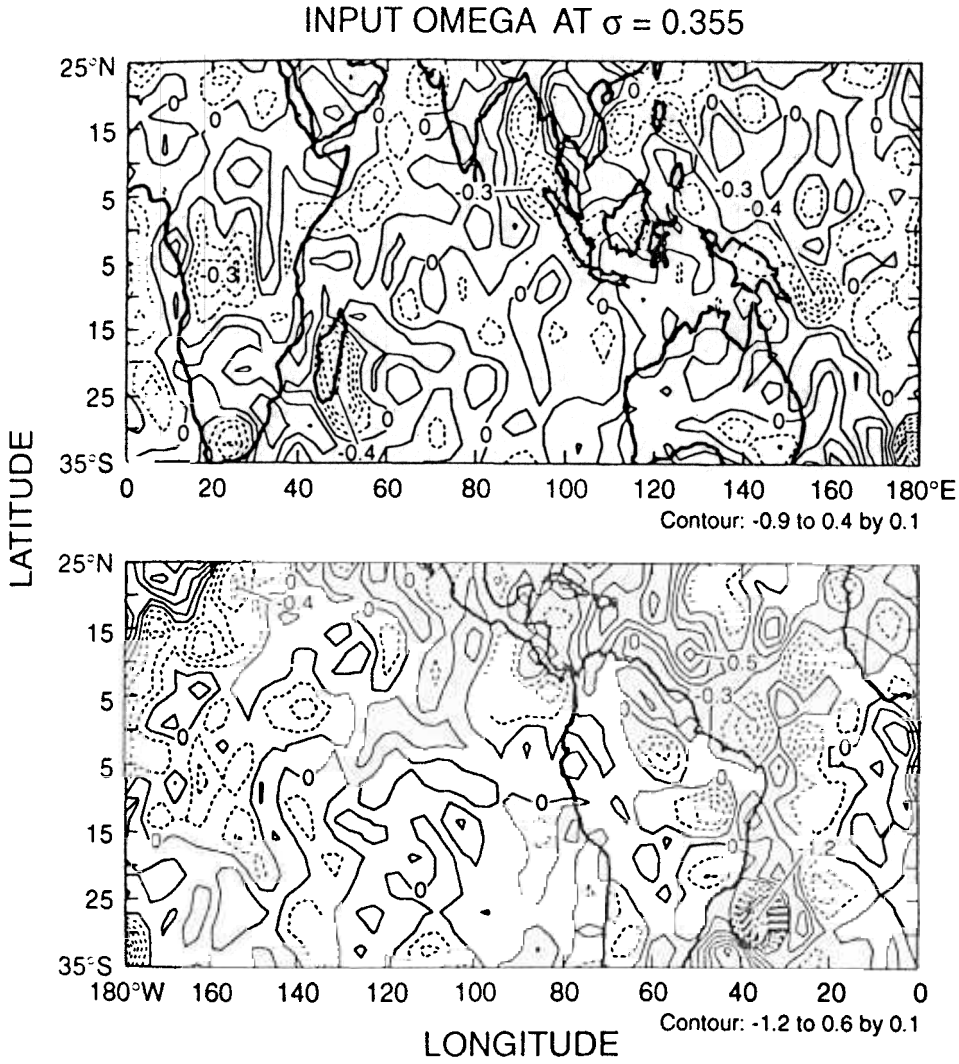

Fig. 3. Input vertical p-velocity at sigma level $\sigma = 0.355$ for 1200 UTC January 1988. Contour interval is 0.1 Pa s

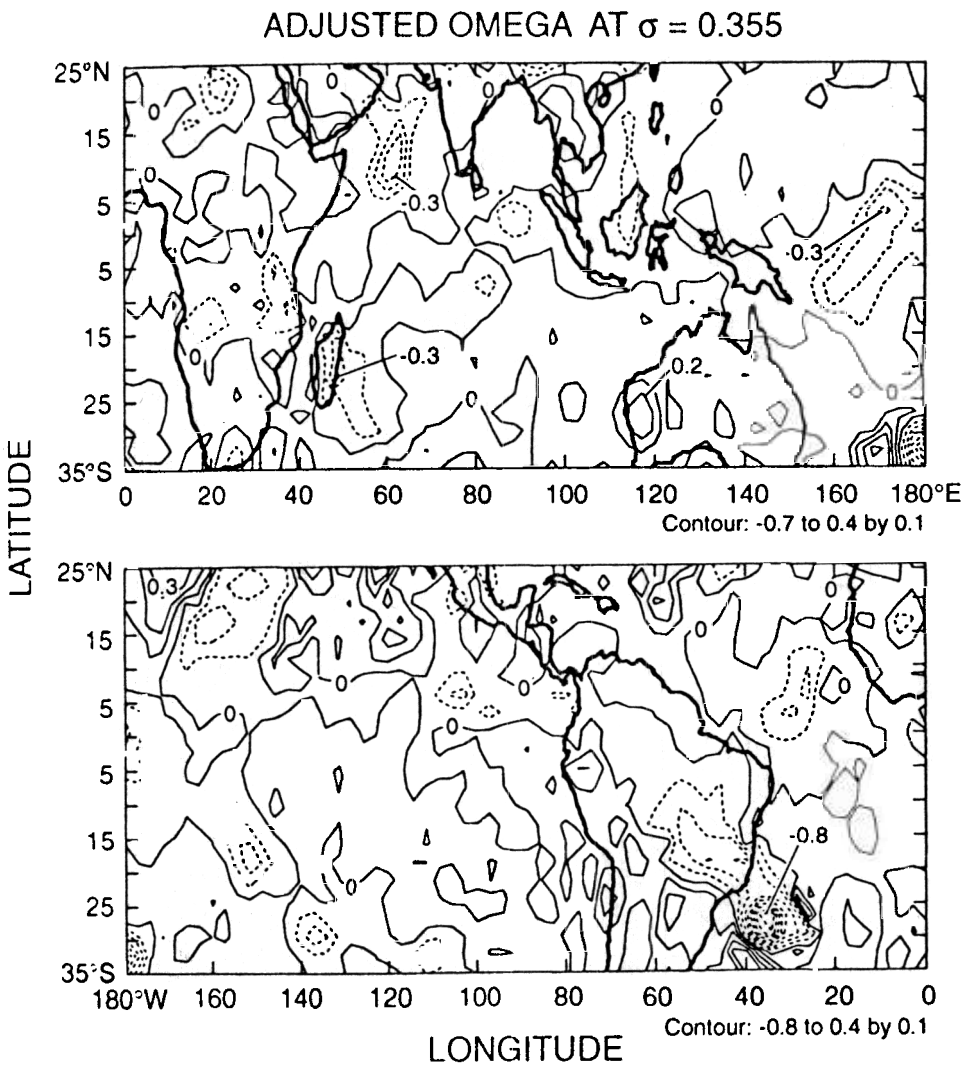

Fig. 4. Adjusted vertical p-velocity at sigma level $\sigma = 0.355$ for 1200 UTC January 1988. Contour interval is same as in Fig. 3.

level. Here, we find that the adjusted ω-field is smoother than the input ω-field of Fig. 3. Moreover, we see good correspondence between the areas of precipitation and upward motion, as well as the organization of convective systems. For example, the convergence zones in the South Pacific and South Atlantic, as well as the convective regions of the western Pacific and Indian Oceans, clearly show organized patterns of ascending motion in Fig. 4.

One unique feature of this adjustment scheme is that it works in both ways to enhance or reduce the magnitudes of D and q depending upon whether the input value I_i is smaller or larger than the observed value I_o. For example, large input ω values over Madagascar and the central Atlantic are now reduced in Fig. 4, while small input ω values over the South Pacific convergence zone are enhanced. Note that the same contour interval is used both in Figs. 3 and 4 to facilitate easier comparison. We see that some upward-motion areas in Fig. 3 are turned to descending motion areas in Fig. 4. For example, strong upward motion over the Bay of Bengal and the Philippines in Fig. 3 is apparently false and is replaced by descending motion. Likewise, descending motion over the eastern South Pacific is enhanced in Fig. 4.

One important observation in Fig. 4 is that the adjustment scheme reduces noise in the downward-motion area of Fig. 3. This is accomplished by the adjustment scheme discussed in Section 4. In fact, it is instructive to compare

Fig. 4 with Fig. 5, which shows the modified ω at $\sigma = 0.355$ after applying the modification of the input ω values only over the descending motion area. The resemblance of Fig. 5 with Fig. 4 is surprisingly good, even though the magnitude of negative p-velocity (ascending motion) in Fig. 5 is different from that in Fig. 4. This indicates that the difficulty looking at the raw analysis of the vertical motion field, such as Fig. 3, is not that the field does not contain the information of reality, but because the vertical motion field is contaminated by noise, particularly in the descending motion area, where the magnitude of vertical velocity is small. The procedure illustrated in deriving Fig. 5 is precisely a means of quality check that should be performed on the first-guess field in data assimilation when the information of convective activity, such as Fig. 2, is available. Unlike the fields of temperature and streamfunction, the vertical motion field is dominated by small-scale motions. Because of this nature it is customary to examine the fields of temperature and streamfunction, and one tends to be reluctant even to look at the vertical motion field. While this practice is acceptable for mid-latitude circulations, we can no longer ignore a careful examination of the vertical motion field in the tropics. Even though there may be room for improvement in the illustration of Figs. 3 to 5, the authors find an important lesson to be learned in showing these figures.

Now the diabatic initialization scheme, however, not only adjusts the divergence field, but

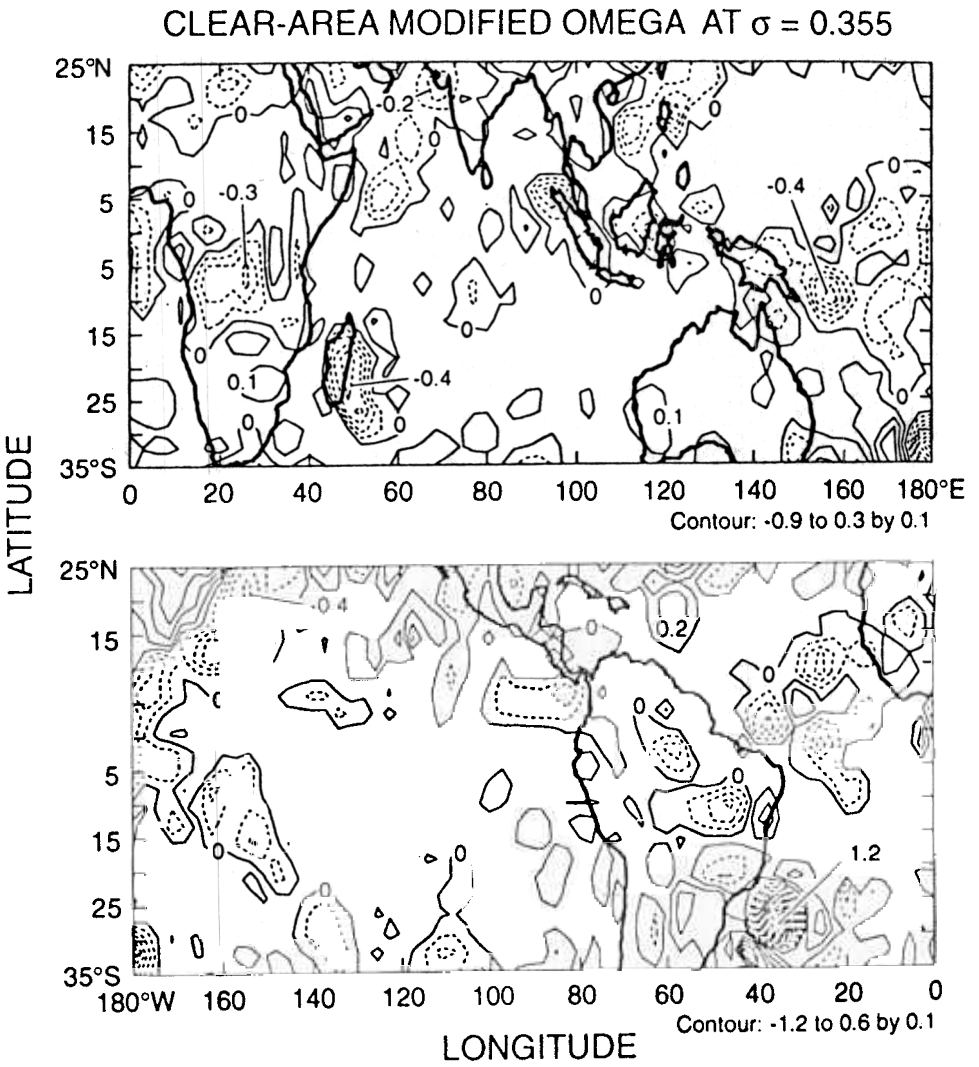

Fig. 5. Clear-area modified p-velocity at sigma level $\sigma = 0.355$ for 1200 UTC 1 January 1988. Contour interval is same as in Fig. 3.

also improves the moisture field for initiation of cumulus convection as we address below.

6.5. *Geographical distribution of precipitable water*

Fig. 6 shows the distribution of input precipitable water, defined by the integral of specific humidity q_i with respect to σ between $\sigma = 1$ and 0.355, for 1200 UTC 1 January 1988. This figure should be compared with Fig. 7, which shows the distribution of adjusted precipitable water at the same time. We see an enhancement of q in the convective area, while q remains unchanged in the convective fringe and downward-motion areas. In this adjustment we imposed a constraint that the adjusted precipitable water be bounded between the input precipitable water and the saturated precipitable water. If we had "observed" precipitable water, this information could be used for (3.18).

Although the input distribution (Fig. 6) shows the signature of convective systems to some degree, such as the South Pacific and Atlantic convergence zones, it fails to capture the convective systems in areas of sparse data coverage, such as the Arabian Sea, Indian Ocean, and mid-Atlantic. By design the adjusted moisture field shown in Fig. 7 is well correlated with the precipitation distribution of Fig. 2.

6.6. *Vertical profiles of meteorological variables at selected points*

Fig. 8a shows the vertical distribution of the input large-scale temperature T_i and cloud temperature T_c calculated from (3.2) and (3.3) at a

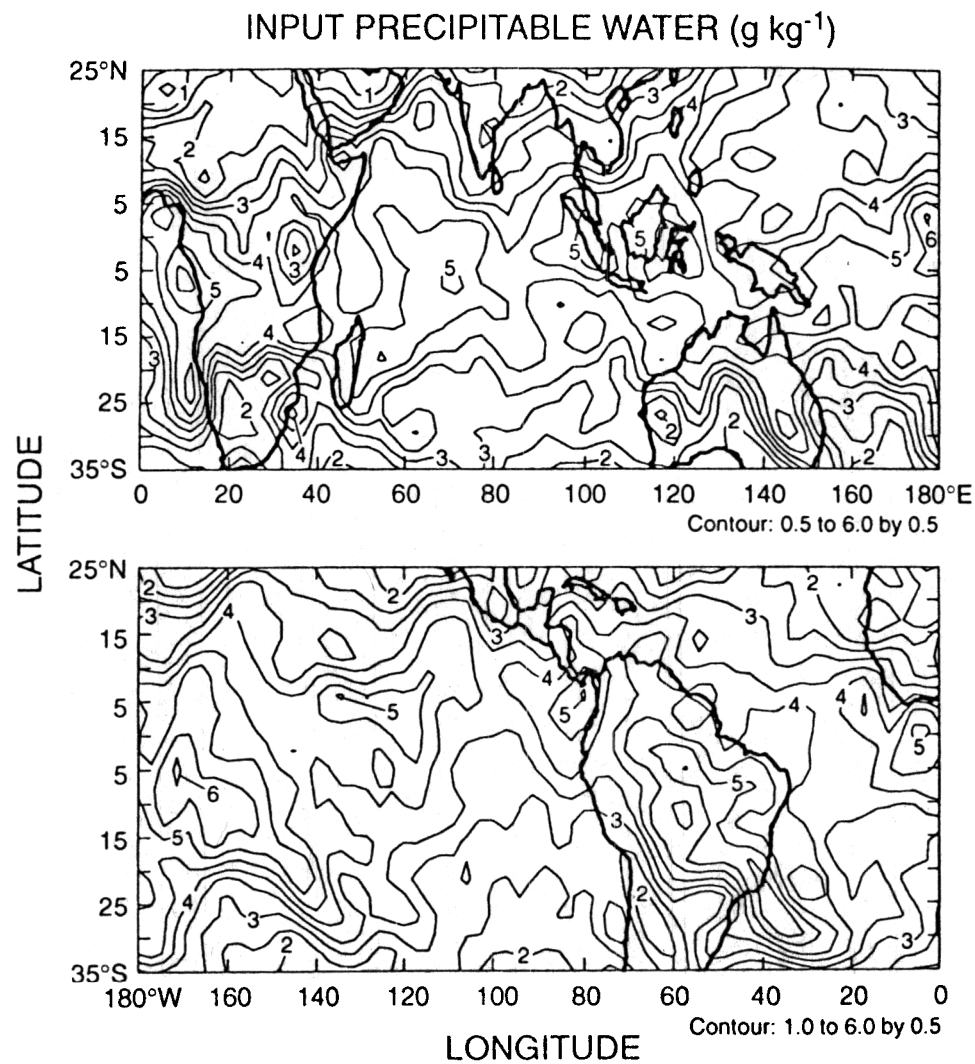

Fig. 6. Input precipitable water distribution for 1200 UTC 1 January 1988. Contour interval is 0.5 g kg

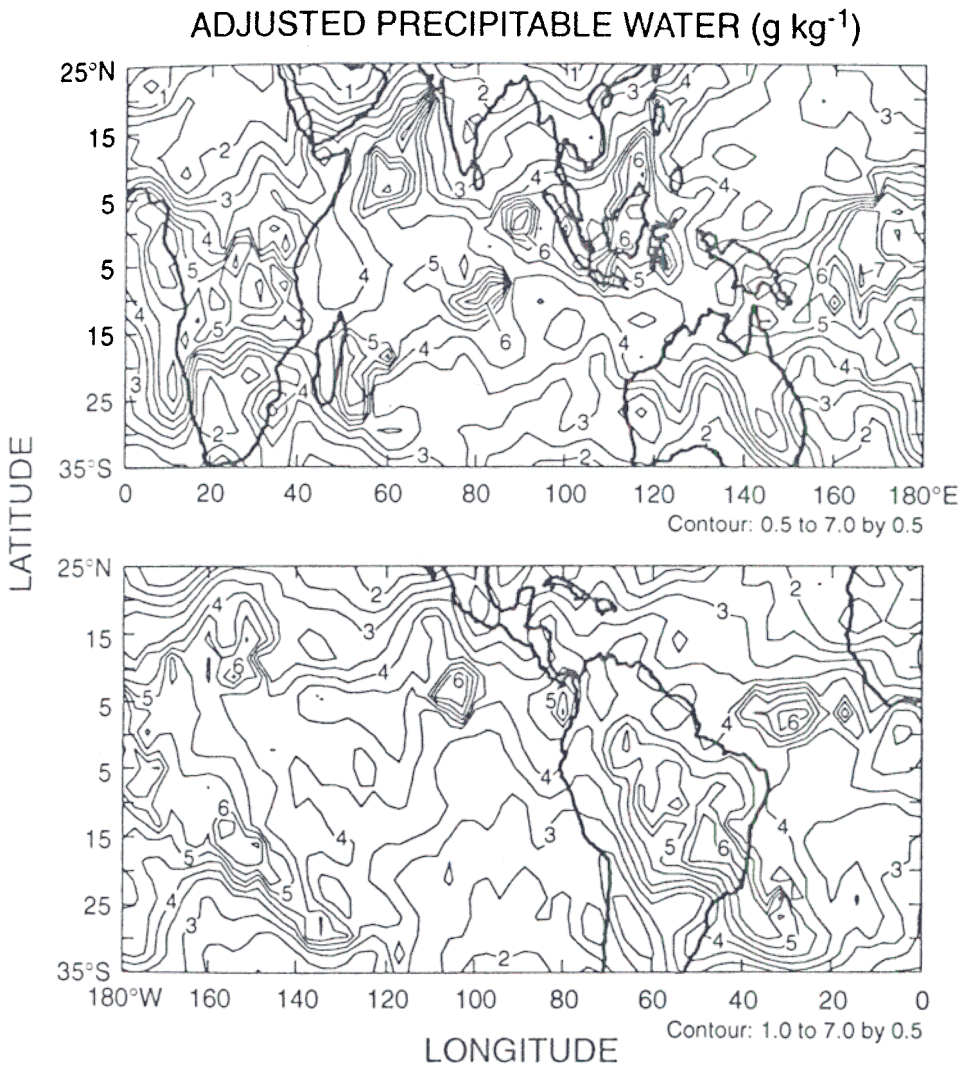

Fig. 7. Adjusted precipitable water distribution for 1200 UTC January 1988. Contour interval is same as in Fig. 6.

convective grid point in the western Pacific. Fig. 8b is the same as Fig. 8a, except it is for input large-scale specific humidity q_i and cloud specific humidity q_c. These are representative vertical profiles of a cumulus cloud and its environment at a convective point.

Fig. 9 shows the vertical distribution of (a) the input divergence D_i and the adjusted value D_a, (b) the input specific humidity q_i, the adjusted value q_a, and the saturation specific humidity q_{sat} corresponding to T_i, (c) the input vertical p-velocity ω_i and the adjusted value ω_a, and (d) the diabatic heating rate as the sum of the convective heating rate Q_c and the radiative heating Q_R. This is an example of a case where the input D_i and the associated ω_i are rather intense and produce a convective heating rate of 10.4 K day^{-1}, while the observed value I_o is 4.8 K day^{-1}. Therefore, the input divergence is reduced to yield less convective heating. In this example, most of the adjustment takes place in the divergence and changes to the specific humidity are small.

At another convective point in the western Pacific, the situation is reversed, namely, the input data produce convective heating of 0.7 K day^{-1}, while the observed value I_o is 5.8 K day^{-1}. A figure (not shown) of vertical distributions similar to Fig. 9 shows that the input divergence is too weak, and there is descending motion in the lower troposphere. In this case, the adjustment scheme increases both the divergence and the specific humidity. For both of these cases, the vertical profiles of convective heating are consistent with the diagnosed heating in tropical mesoscale

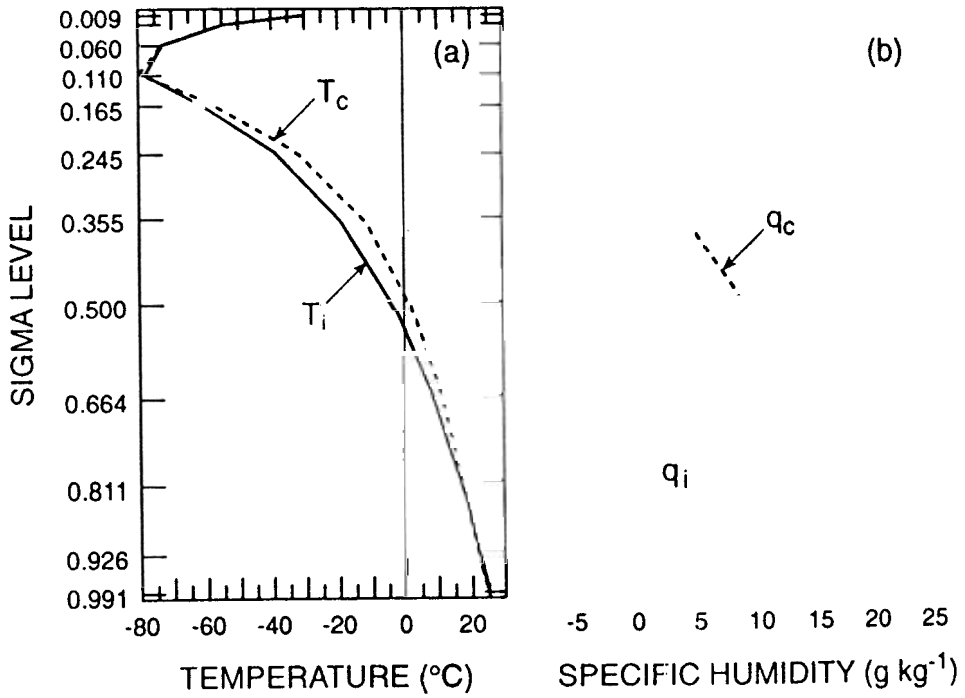

Fig. 8. (a) Vertical distributions of input large-scale temperature T_i and cloud temperature T_c at longitude 154.7° E and latitude 9.8° S. (b) Same as (a) except for input large-scale specific humidity q_i and cloud specific humidity q_c.

convective systems shown by Houze (1982) and Johnson and Young (1983).

6.7. *Mean vertical profiles of divergence and specific humidity in convective, convective fringe, and downward-motion areas*

As mentioned, the tropical belt from 35° S to 25° N is divided into three parts: convective, convective fringe, and downward-motion areas. Fig. 10 shows the mean vertical profiles of (a) the input divergence D_i and the adjusted D_a, (b) the input vertical p-velocity ω_i and the adjusted ω_a, and (c) the input specific humidity q_i and the adjusted q_a, averaged over the part of convective area where the observed heating rate I_o is greater than 5 K day^{-1}. In comparison with D_i and ω_i, the adjustment procedure has yielded stronger divergence in the upper troposphere and increased lower tropospheric convergence in general, producing stronger upward motion. The mean vertical profiles of adjusted D_a and ω_a in Fig. 10 resemble the vertical profiles of divergence and vertical p-velocity shown in Fig. 11 for cloud clusters over the western Pacific obtained by Ruprecht and Gray (1976). It is reasonable to compare our results with those of the western Pacific rather than the West Indies, where the intensities of divergence and vertical p-velocity are relatively weak, since our results are dominated by Pacific convective areas. Our adjustment procedure increased the specific humidity throughout the troposphere, except at the level $\sigma = 0.926$, where q_a became smaller than q_i. The same feature appears in the example shown by Donner (1988) and the initialization experiment described by Kasahara et al. (1992). This feature combined with the observation that ω_a in the lower troposphere is relatively small will contribute to reduce stable precipitation as determined by the oversaturation of an air parcel (see Section 4r on stable condensation in Williamson et al., 1987). This may be a desirable feature in precipitation forecasts for the tropics where convective precipitation may dominate over stable precipitation.

We have prepared a figure (not shown) similar to Fig. 10, except that averaging is taken over the convective points where the observed heating rate I_o is less than 5 K day^{-1}. It is reasonable to expect that the profiles of D_a and ω_a are weaker than those shown in Fig. 10. Moreover, the profiles of D_a and ω_a show good agreement with those of D_i and ω_i, indicating that the original ECMWF analysis reflects the realism of convective distribution in the region of relatively weaker convective

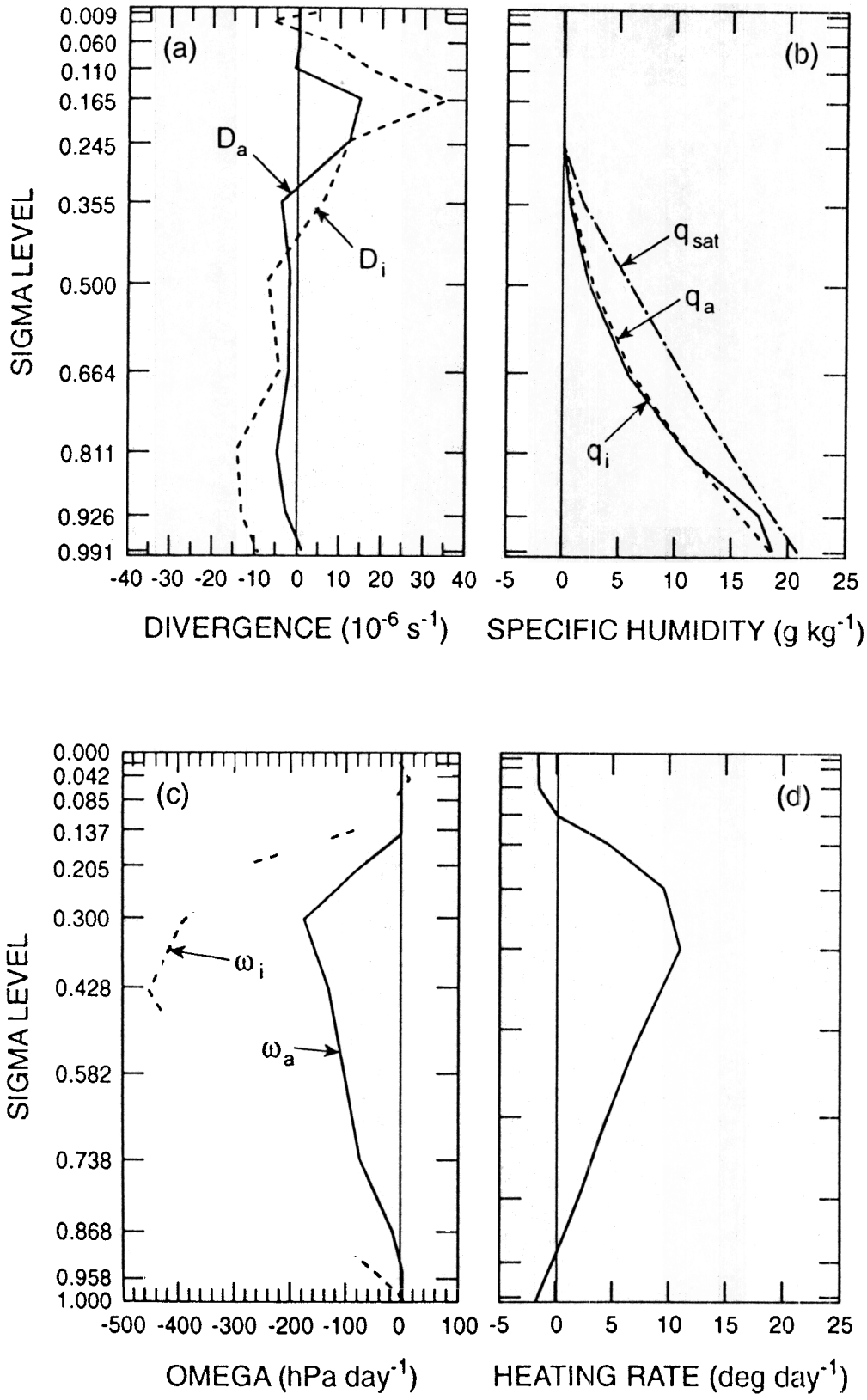

Fig. 9. Vertical distributions of various meteorological variables at longitude 154.7° E and latitude 9.8° S. (a) Input divergence D_i and adjusted value D_a, (b) input specific humidity q_i, adjusted value q_a, and saturated specific humidity q_{sat}, (c) input vertical p-velocity ω_i and adjusted value ω_a, and (d) diabatic heating rate.

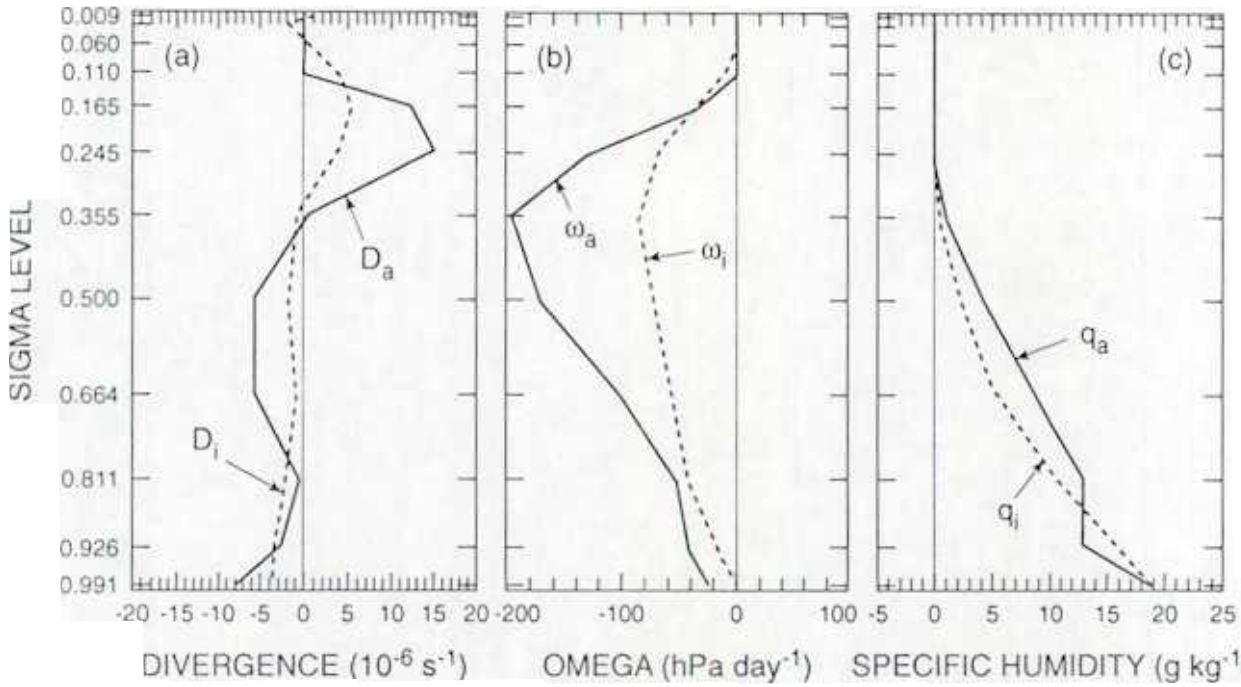

Fig. 10. Mean vertical distributions of (a) input divergence D_i and adjusted value D_a, (b) input vertical p-velocity ω_i and adjusted value ω_a, and (c) input specific humidity q_i and adjusted value q_a, all averaged over the convective points where the observed heating I_o is greater than 5 K day^{-1} in the convective area.

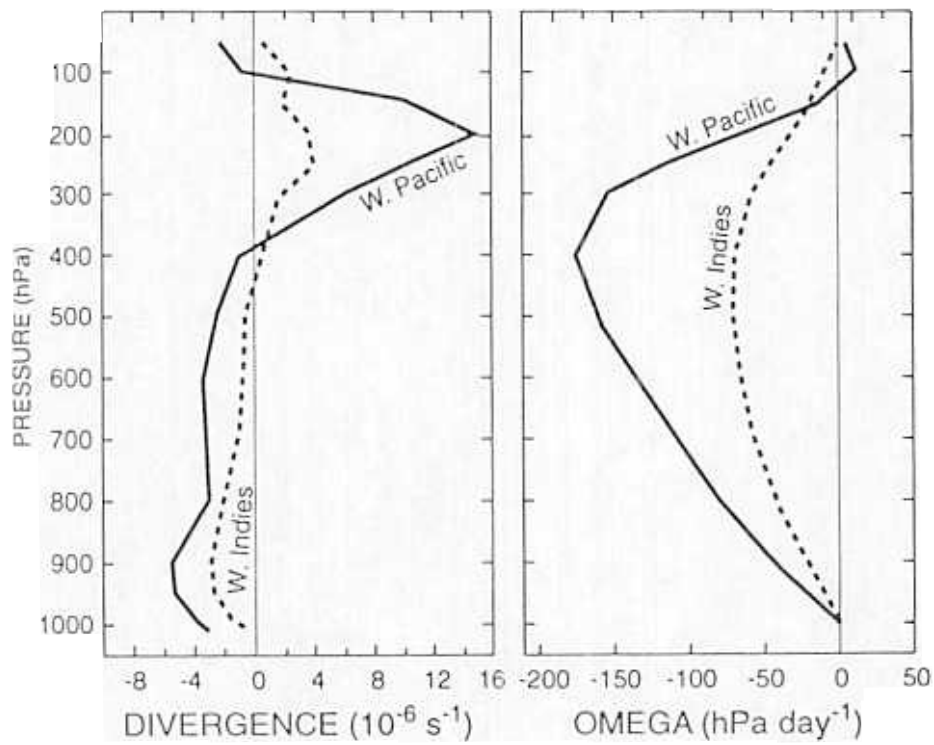

Fig. 11. Mean vertical profiles of divergence (left panel) and vertical p-velocity (right panel) for Western Pacific and West Indies cloud clusters (adopted from Ruprecht and Gray, 1976).

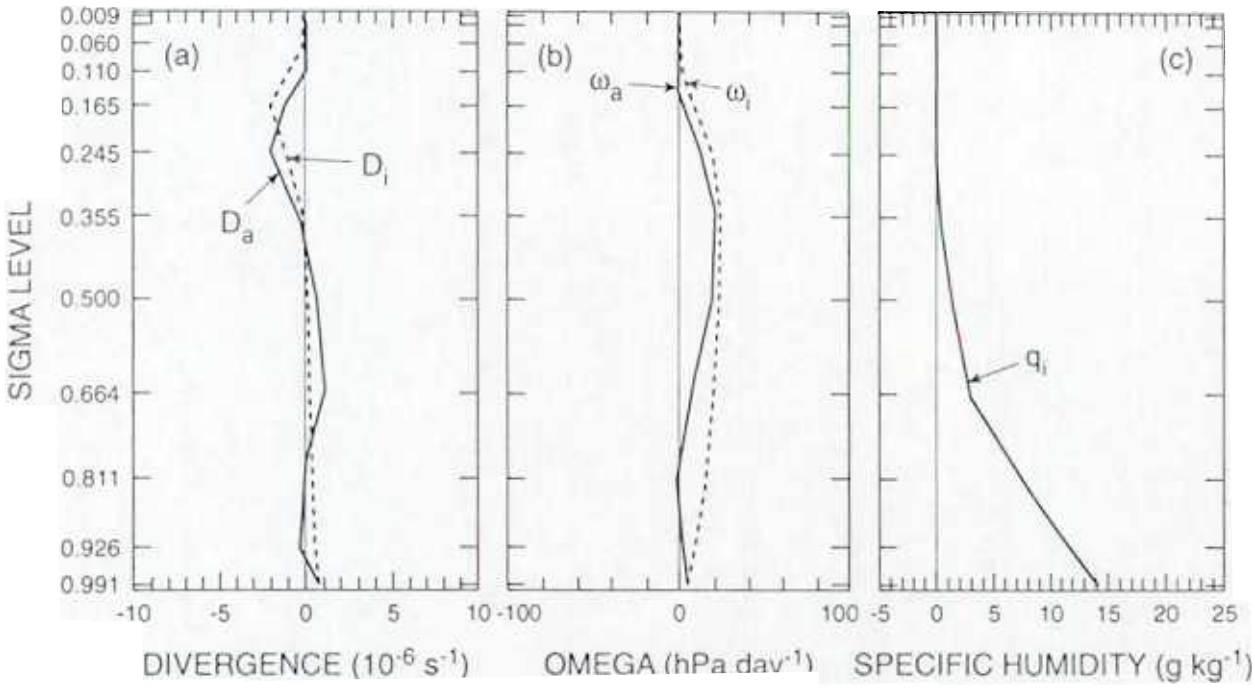

heating. However, the adjusted q_a has increased over q_i, except for the level $\sigma = 0.926$. Again, this feature is consistent with the changes to the moisture profile q_a shown in Fig. 10.

Fig. 12 is the same as Fig. 10, except that averaging is taken over the downward-motion area. Note that no adjustment was made for q_i. It is reasonable to expect that air is much drier on average in the downward-motion area than in the convective region. Again, we see generally good agreement between ω_i and ω_a, as well as D_i and D_a. Apparently, the averaging smoothed out

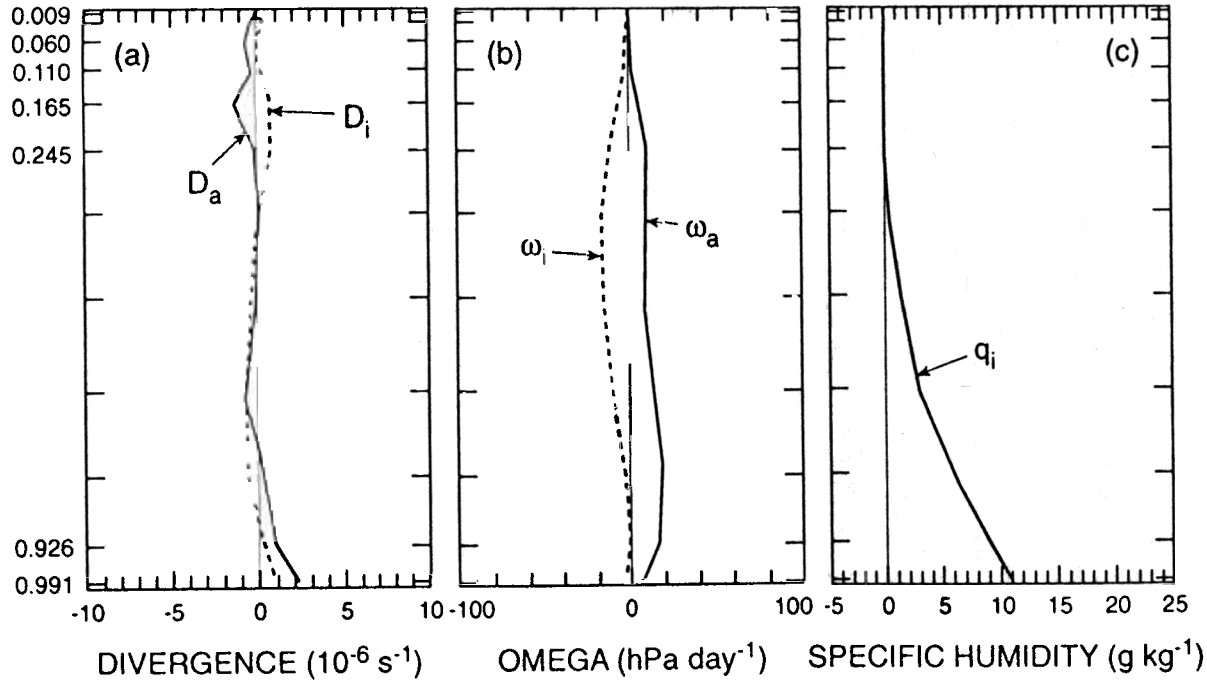

Fig. 13. Same as Fig. 10, except that averaging is taken over the convective fringe area.

small-scale noise in the input divergence field and produced mean profiles of D_i and ω_i, which are very similar to D_a and ω_a.

Fig. 13 is the same as Fig. 10, except that the averaging is taken over the convective fringe area. Again, no adjustment is made for q_i, and air in this area is even drier than the downward-motion area shown in Fig. 12. The change in the profile of D_i to produce D_a occurs as the result of applying the global conservation of D discussed in Section 5. Since the magnitude of ω_a in the intense convective area has increased as seen in Fig. 10, it is reasonable to expect that its compensation takes place in the convective fringe area, and weak upward motion is changed to weak downward motion. The observation that weak downward motion prevails in the convective fringe area is not inconsistent with the fact that air in this area is even drier than the downward-motion area.

7. Concluding remarks

Atmospheric data assimilation, which consists of blending observations with first-guess fields, is similar to team work in that its quality is influenced by the weakest member of the group. In other words, it is most cost effective to improve analysis techniques in the area of the greatest weakness. As pointed out in Section 2, the quality of the daily analysis of horizontal divergence and moisture fields in the tropics is deficient. Thus, we can improve the global analyses by improving the tropical analyses through the synergistic effect produced by the forecast-analysis cycle of the four-dimensional data assimilation and the teleconnection couplings between the tropics and the rest of the globe.

In this article, we propose a diabatic initialization scheme to improve the analysis of horizontal divergence and humidity fields in the tropics by incorporating information on the convective activity and proxy data for precipitation obtained from satellite radiometric imagery data. This adjustment scheme is used for the physical initialization of cumulus convection in the initial conditions for a global prediction model. Also, this scheme may be used as a means of quality control for the first-guess fields of horizontal divergence, moisture, and temperature in four-dimensional data assimilation systems. The effectiveness of this algorithm in practice depends on two factors. One is the reliability of the cumulus parameterization used as a physical model to represent reality. The other is the accuracy of precipitation estimates obtained from satellite data.

As far as the cumulus parameterization is concerned, we adopted the Kuo cumulus parameterization as described by Donner et al. (1982). The scheme has been incorporated in the version of CCM1 that was used in diabatic initialization experiments of Donner and Rasch (1989) and Kasahara et al. (1992). Since the initialization is based on the inversion of cumulus parameterization and an optimization technique is used to solve the inversion process, it is necessary to use the same cumulus parameterization in the initialization procedures as that in the prediction model. This same principle of adjustment should be applicable to different cumulus parameterizations as long as explicit formulae are used to relate the convective heating or precipitation rate to the divergence or vertical velocity and moisture fields.

The accuracy of satellite precipitation estimates is an important question, since the quality of adjusted divergence and moisture fields depends critically on the input data, as well as the procedure of optimization for solving the inversion process of cumulus parameterization. The satellite-derived information, such as convective patterns and precipitation rates, is unique in that the quantitative aspects of information, such as the magnitude of the precipitation rate, are less reliable than the qualitative aspects of information, such as the location of rainfall and the relative magnitude of the precipitation rate. Therefore, we must be prepared to apply a correction to the magnitude of proxy precipitation rate so that the associated heating rate produces dynamical and thermodynamical motions of reasonable magnitudes in the prediction model. The reduction of the OLR-based convective heating rate I_o, as discussed in Subsection 6.1, is applied to produce an adjusted divergence field whose average magnitudes agree with the input divergence field. Ultimately, the magnitude of the correction should be decided by forecast experiments so that the mean precipitation rate produced by the model climatology and that inferred from the satellite data are consistent. This will be the topic of a further study.

8. Acknowledgments

Partial support for this research has been provided by NOAA Grant NA88AANG 0140 and NASA Grant NAG 8-809. The authors thank two anonymous reviewers for their comments to improve the manuscript.

9. Appendix

To derive the constraint (3.20), we perform a scale analysis in the tropics using a baroclinic primitive equation model on an equatorial β-plane expressed in the form:

$$\frac{\hat{c}\boldsymbol{V}}{\hat{c}t}+\boldsymbol{V}\cdot\nabla\boldsymbol{V}+\omega\frac{\hat{c}\boldsymbol{V}}{\hat{c}p}+\beta y\boldsymbol{k}\times\boldsymbol{V} = -\nabla\Phi+\boldsymbol{F}, \tag{A.1}$$

$$\frac{\hat{c}\Phi}{\hat{c}p}=-\frac{RT}{p}, \tag{A.2}$$

$$\nabla\cdot\boldsymbol{V}+\frac{\partial\omega}{\partial p}=0, \tag{A.3}$$

$$\left(\frac{\hat{c}}{\partial t}+\boldsymbol{V}\cdot\nabla\right)\frac{\partial\Phi}{\partial p}+\frac{\omega}{p}\frac{\hat{c}}{\partial p}\left(p\frac{\partial\Phi}{\partial p}-\kappa\Phi\right) = -\frac{\kappa}{p}Q, \tag{A.4}$$

where $\boldsymbol{V}=u\boldsymbol{i}+v\boldsymbol{j}$, $\nabla=\boldsymbol{i}(\partial/\partial x)+\boldsymbol{j}(\hat{c}/\partial y)$ in which $\boldsymbol{i}$ and $\boldsymbol{j}$ denote unit vectors in x and y coordinates, respectively, $\boldsymbol{k}$ denotes a unit vector upward in decreasing pressure, $\beta=\mathrm{d}f/\mathrm{d}y$ with f being Coriolis parameter, Φ geopotential, $\kappa=R_\mathrm{d}/C_\mathrm{p}$, $\boldsymbol{F}$ frictional force per unit mass, and Q the time rate of heating per unit mass. Eq. (A.4) is derived from the thermodynamic equation

$$\frac{\mathrm{d}}{\mathrm{d}t}\ln\theta=\frac{Q}{C_\mathrm{p}T},$$

where θ denotes the potential temperature $\theta=T(p_0/p)^\kappa$ with $p_0=1000$ hPa, and the relationship

$$\frac{\partial\Phi}{\partial p}\frac{\partial\ln\theta}{\partial p}=\frac{1}{p}\frac{\partial}{\partial p}\left(p\frac{\partial\Phi}{\partial p}-\kappa\Phi\right) \tag{A.5}$$

with application of the hydrostatic eq. (A.2).

We assume the following magnitudes for the scaling of basic variables of large-scale motions (Charney, 1948).

$$\begin{aligned}
&L\equiv\text{horizontal scale}=\mathrm{O}(10^6)\ \text{m},\\
&H\equiv\text{vertical scale}=\mathrm{O}(10^4)\ \text{m},\\
&P\equiv\text{vertical scale in pressure}\approx 1000\ \text{hPa},\\
&U\equiv\text{horizontal particle speed}=\mathrm{O}(10)\ \text{m s}^{-1}\\
&L/U\equiv\text{scaling of time}=\mathrm{O}(10^5)\ \text{s}.
\end{aligned} \tag{A.6}$$

The order of magnitudes of the parameters related to the earth is assumed to be

$$\begin{aligned}
&g\equiv\text{gravity acceleration}\approx 10\ \text{m s}^{-2},\\
&\Omega\equiv\text{angular speed}\approx 10^{-4}\ \text{s}^{-1},\\
&r\equiv\text{mean radius}\approx 10^7\ \text{m}.
\end{aligned}$$

We introduce the following dimensionless variables denoted by prime:

$$\begin{aligned}
&\boldsymbol{V}'=\boldsymbol{V}/U, && (x',y')=(x,y)/L\\
&t'=UL^{-1}t, && \nabla'=L\nabla\\
&p'=p/P, && \omega'=L(PU)^{-1}\omega.
\end{aligned}$$

We also introduce the scaling for the frictional force $\boldsymbol{F}$ and the heating Q:

$$\boldsymbol{F}'=LU^{-2}\boldsymbol{F},$$

$$Q'=(2\Omega U^2)^{-1}Q,$$

based on the following consideration. The magnitude of $\boldsymbol{F}$ is estimated from the rate of energy dissipation that takes place mainly in the atmospheric boundary layer. Therefore, it is estimated from $|\boldsymbol{F}|\approx C_\mathrm{d}V_\mathrm{s}^2/d\approx 10^{-4}\ \text{m s}^{-2}$ by choosing typical values of the parameters; the drag coefficient $C_\mathrm{d}=10^{-3}$, the surface wind speed $V_\mathrm{s}=10\ \text{m s}^{-1}$, and the boundary layer thickness $d=1000$ m. The magnitude of Q is estimated from $Q\approx C_\mathrm{p}\,\Delta T/\Delta t\approx 10^{-2}\ \text{m}^2\ \text{s}^{-3}$ by choosing $\Delta T/\Delta t$ to be of the order of 1 K day^{-1} for large-scale diabatic heating/cooling by radiation and the release of latent heat of condensation.

The scaling of Rossby parameter β is chosen to be

$$\beta y=(2\Omega)\,R_1\,y \tag{A.10}$$

and

$$R_1 = L/r = O(10^{-1}),$$

using (A.6) and (A.7).

The scaling of the geopotential Φ is chosen to be

$$\Phi = gH\Phi'_s(p) + (2\Omega UL)\, R_0\Phi'$$
$$R_0 = U/(2\Omega L) = O(10^{-1}), \tag{A.11}$$

where $\Phi'_s(p)$ denotes a dimensionless geopotential of the standard atmosphere, which depends only on p, Φ' is a dimensionless geopotential deviation, and R_0 denotes the Rossby number. The reasoning of the scaling $(2\Omega UL)\, R_0$ for Φ' will be explained later.

By introducing these scaling considerations into (A.1), we can now write the dimensionless equation of motion as

$$\frac{\partial V'}{\partial t} + V'\cdot\nabla' V' + \omega'\frac{\partial V'}{\partial p} + \left(\frac{R_1}{R_0}\right) y' k \times V' = -\nabla'\Phi' + F' \tag{A.12}$$

Note that $R_1/R_0 = O(1)$ that will be denoted as β'. Therefore, all the terms of (A.12) are on the same order of magnitude. In fact, the coefficient $(2\Omega UL)\, R_0$ for Φ' is chosen so that the pressure gradient $\nabla\Phi$ and the Coriolis force term $\beta y k \times V$ have the same order of magnitude. The result is that $(2\Omega UL)\, R_0 = O(10^2)$ m s^{-2}, which is appropriate as the order of magnitude of the deviation Φ from the standard atmosphere in the tropics. The observation that all the terms of (A.12) are on the same order of magnitude clearly indicates the complicated nature of equatorial dynamics, due to the lack of a simple balance, compared with the large-scale quasi-geostrophic motions in the mid-latitudes.

By applying the operator ∇' to (A.12), we obtain the dimensionless horizontal divergence equation in the form:

$$\frac{\partial D'}{\partial t'} + V'\cdot\nabla' D' + \omega'\frac{\partial}{\partial p} D' + \nabla'\omega'\frac{\partial V'}{\partial p} + D'^2 - 2J(u', v') - \beta' y'\zeta' + \beta' u' = -\nabla'^2\Phi' + \nabla'\cdot F', \tag{A.13}$$

where

$$D' = \nabla'\cdot V', \qquad \zeta' = k\cdot\nabla'\times V',$$
$$J(u', v') = u'_x v'_y - u'_y v'_x.$$

Since convective regions are characterized by a lower level convergence and upper level divergence, the intensity of convection may be measured by the derivative $\partial D'/\partial p'$. When convection is developing rather rapidly with respect to time, the second derivative $\partial^2(\partial D'/\partial p')/\partial t'^2$ must be large in magnitude, even though the first derivative $\partial(\partial D'/\partial p')/\partial t'$ is small. Therefore, to control the overshooting of D' with respect to time, it is essential to ensure that both the first and second derivatives of $\partial D'/\partial p'$ with respect to time are sufficiently small. This consideration permits the coupling of the dynamics represented by (A.13) with the thermodynamic eq. (A.4), which is now written in the following dimensionless form:

$$\left(\frac{\partial}{\partial t'} + V'\cdot\nabla'\right)\frac{\partial\Phi'}{\partial p'} + \omega'\left[R_i + \frac{1}{p'}\frac{\partial}{\partial p'}\times\left(p'\frac{\partial\Phi'}{\partial p'} - \kappa\Phi'\right)\right] = -R_0^{-1}\frac{\kappa}{p'}Q', \tag{A.14}$$

where R_i denotes a Richardson number defined as

$$R_i = \frac{gH}{RT^2}\frac{d\Phi'_s}{dp'}\frac{d\ln\theta_s}{dp'} = O(10^2)$$

by application of (A.6), (A.7), and taking into account $d\ln\theta_s/dp' = O(10^{-1})$.

Thus, we get, *after dropping all primes* for simplicity,

$$\frac{\partial}{\partial p}\left(\frac{\partial^2 D}{\partial t^2}\right) = -\frac{\partial}{\partial t\,\partial p}\left[V\cdot\nabla D + D^2 + \nabla\left(\omega\cdot\frac{\partial V}{\partial p}\right)\right] + \frac{\partial}{\partial t\,\partial p}\left[2J(u, v) + \beta y\zeta - \beta u + \nabla\cdot F\right] + \nabla^2\left[V\cdot\nabla\left(\frac{\partial\Phi}{\partial p}\right) + \omega R_i + \frac{\omega}{p}\frac{\partial}{\partial p}\times\left(p\frac{\partial\Phi}{\partial p} - \kappa\Phi\right) + R_0^{-1}\frac{\kappa Q}{p}\right] \tag{A.15}$$

A noteworthy point in the above equation is that the second and fourth terms in the last set of square brackets are one to two orders of magnitude larger than the rest of the terms. This implies that these two terms must cancel each other to have relevant scales of motion. This leads to the requirement that

$$\omega R_i + R_0^{-1}\frac{\kappa Q}{p} = O(\qquad \text{(A.16)}$$

Moreover, since $R_i = O(10^2)$ and $R_0 = O(10^{-1})$, this relationship suggests

$$\omega = O(R_0) \quad \text{and} \quad D = O(R_0) \qquad \text{(A.17)}$$

with application of the continuity eq. (A.3).

The important conclusion here is that the vertical circulations in the tropics are basically thermal-driven everywhere, including both convective and nonconvective areas. This conclusion has been noted earlier by Holton (1972) who said that "the synoptic scale vertical motion, and hence the divergence field, can be diagnostically computed if the synoptic scale distribution of diabatic heating is known." The scaling of ω and D shown by (A.17) in the tropics is the same as that in the mid-latitudes, as discussed by Charney (1948). It is important to point out, however, that the mid-latitude scaling of ω or D is due to geostrophic balance, while the tropical scaling of ω or D is the consequence of thermal balance.

With this refinement of the scaling of ω and D, and neglecting the terms of order R_0 or smaller, (A.15) is expressed by

$$\frac{\partial}{\partial p}\left(\frac{\partial^2 D}{\partial t^2}\right) = \frac{\partial}{\partial t\,\partial p}\left[2J(u, v) + \beta y\zeta - \beta u + \nabla\cdot\boldsymbol{F}\right] + \nabla^2\left[\boldsymbol{V}\cdot\nabla\left(\frac{\partial\Phi}{\partial p}\right) + \left(\omega R_0 R_i + R_0^{-1}\frac{\kappa Q}{p}\right)\right] \qquad \text{(A.18)}$$

with the incorporation of the balance requirement (A.16).

To control the fast growth of horizontal divergence associated with the problem of precipitation spinup, we need to ensure not only that $\partial D/\partial t$ is on the order of R_0, but also that $\partial^2(\partial D/\partial p)/\partial t^2$ is on the order of R_0. Assuming that the following balance requirement, which ensures $|\partial D/\partial t| = O(R_0)$ with reference to (A.13),

$$2J(u, v) + \beta y\zeta - \beta u - \nabla^2\Phi + \nabla\cdot\boldsymbol{F} = O(R_0)$$

is satisfied, the condition that $|\partial^2(\partial D/\partial p)/\partial t^2|$ be kept on the order of R_0 in (A.18) provides a means of further refinement of ω beyond its first approximation achieved by (A.16).

REFERENCES

Arkin, P. A. and Meisner, B. N. 1987. The relationship between large-scale convective rainfall and cold cloud over the Western Hemisphere during 1982–1984. *Mon. Wea. Rev.* **115**, 51–74.

Baba, A. 1987. Improvement of the estimation method of moisture data from satellite cloud soundings. *JMA/NPD Tech. Rep. No. 16*, 54 pp. (Available from Numerical Prediction Division, Japan Meteorological Agency, Ote-machi, Chiyoda-ku, Tokyo 100, Japan.)

Charney, J. G. 1948. On the scale of atmospheric motions. *Geophys. Publ.* **17**, 17 pp.

Daley, R. 1991. *Atmospheric data analysis.* Cambridge University Press, Cambridge, MA, 457 pp.

Donner, L. J. 1988. An initialization for cumulus convection in numerical weather prediction models. *Mon. Wea. Rev.* **116**, 377–385.

Donner, L. J. and Rasch, P. J. 1989. Cumulus initialization in a global model for numerical weather prediction. *Mon. Wea. Rev.* **117**, 2654–2671.

Donner, L. J., Kuo, H.-L. and Pitcher, E. J. 1982. The significance of thermodynamic forcing by cumulus convection in a general circulation model. *J. Atmos. Sci.* **39**, 2159–2181.

Heckley, W. A., Kelly, G. and Tiedtke, M. 1990. On the use of satellite-derived heating rates for data assimilation within the tropics. *Mon. Wea. Rev.* **118**, 1743–1757.

Hollingsworth, A., Horn, J. and Uppala, S. 1989. Verification of FGGE assimilations of the tropical wind field: The effect of model and data bias. *Mon. Wea. Rev.* **117**, 1017–1038.

Holton, J. R. 1972. *An introduction to dynamic meteorology*, 1st edition. Academic Press, 319 pp.

Houze, Jr., R. A. 1982. Cloud clusters and large-scale vertical motions in the tropics. *J. Meteor. Soc. Japan* **60**, 396–410.

Illari, L. 1987. *The "spin-up" problem.* Technical Memo No. 137, ECMWF, Reading, United Kingdom.

Janowiak, J. E. and Arkin, P. A. 1991. Rainfall variations in the tropics during 1986–1989, as estimated from observations of cloud-top temperature. *J. Geophy. Res.* **96**, supplement, 3359–3373.

Johnson, R. H. and Young, G. S. 1983. Heat and moisture budgets of tropical mesoscale anvil clouds. *J. Atmos. Sci.* **40**, 2138–2147.

Julian, P. A. 1984. Objective analysis in the tropics: A proposed scheme. *Mon. Wea. Rev.* **112**, 1752–1767.

Kasahara, A., Balgovind, R. C. and Katz, B. B. 1988. Use of satellite radiometric imagery data for improvements in the analysis of divergent wind in the tropics. *Mon. Wea. Rev.* **116**, 866–883.

Kasahara, A. and Mizzi, A. P. 1992. Estimates of tropical analysis differences in daily values produced by two operational centers. *Mon. Wea. Rev.* **120**, 279–302.

Kasahara, A., Mizzi, A. P. and Donner, L. J. 1992. Impact of cumulus initialization on the spinup of precipitation forecasts in the tropics. *Mon. Wea. Rev.* **120**, 1360–1380.

Kasahara, A., Mizzi, A. P. and Mohanty, U. C. 1987. Comparison of global diabatic heating rates from FGGE Level IIIb analyses with satellite radiation imagery data. *Mon. Wea. Rev.* **115**, 2904–2935.

Krishnamurti, T. N., Xue, J., Bedi, H. S., Ingles, K. and Oosterhof, D. 1991. Physical initialization for numerical weather prediction over the tropics. *Tellus* **43AB**, 53–81.

Krishnamurti, T. N., Bedi, H. S., Heckley, W. and Ingles, K. 1988. Reduction of the spinup time for evaporation and precipitation in a spectral model. *Mon. Wea. Rev.* **116**, 907–920.

Krishnamurti, T. N., Ingles, K., Cocke, S., Kitade, T. and Pasch, R. 1984. Details of low latitude medium range numerical weather prediction using a global spectral model. Part II. Effects of orography and physical initialization. *J. Meteor. Soc. Japan* **62**, 613–649.

Kuo, H.-L. 1974. Further studies of the influence of cumulus convection on large-scale flow. *J. Atmos. Sci.* **31**, 1232–1240.

Lambert, S. J. 1989. A comparison of divergent winds from the National Meteorological Center and the European Center for Medium-Range Weather Forecasts global analyses for 1980–1986. *Mon. Wea. Rev.* **117**, 995–1005.

Mathur, M. B., Bedi, H. S., Krishnamurti, T. N., Kanamitsu, M. and Woollen, J. S. 1992. Use of satellite-derived rainfall for improving tropical forecasts. *Mon. Wea. Rev.* **120**, 2540–2560.

Mayer, T. A. 1988. Generation of CCM format history tapes from analyzed data for selected periods (RD2CFM Version 01). *Technical Note NCAR/TN-322 + IA*, NCAR, Boulder, CO, 68 pp.

Mills, G. A. and Davidson, N. E. 1987. Tropospheric moisture profiles from digital IR satellite imagery: System description and analysis/forecast impact. *Aust. Meteor. Mag.* **35**, 109–118.

Mizzi, A. P. and Kasahara, A. 1989. Intercomparison of daily values of atmospheric variables, including diabatic heating rates, from the ECMWF, GFDL, and Goddard Laboratory for Atmospheres FGGE Level IIIb analyses. *J. Geophys. Res.* **94**, 14717–14748.

Pasch, R. and Illari, L. 1985. FGGE moisture analysis and assimilation in the ECMWF system. *ECMWF Tech. Memo No. 110*, 25 pp. (Available from ECMWF, Shinfield Park, Reading, Berkshire, RG2 9AX, United Kingdom.)

Puri, K. and Miller, M. J. 1990. The use of satellite data in the specification of convective heating for diabatic initialization and moisture adjustment in numerical weather prediction. *Mon. Wea. Rev.* **118**, 67–93.

Puri, K. and Davidson, N. E. 1992. The use of infrared satellite cloud imagery data as proxy data for moisture and diabatic heating in data assimilation. *Mon. Wea. Rev.* **120**, 2329–2341.

Ruprecht, E. and Gray, W. M. 1976. Analysis of satellite-observed tropical cloud clusters. I. Wind and dynamic fields. *Tellus* **28**, 391–411.

Spencer, R. W., Goodman, H. M. and Hood, R. E. 1989. Precipitation retrieval over land and ocean with the SSM/I: Identification and characteristics of the scattering signal. *J. Atmos. Oceanic Tech.* **6**, 254–273.

Theon, J. and Fugono, N. 1988. *Tropical rainfall measurements*. A. Deepak Publishers, Hampton, Virginia, 523 pp.

Thompson, Jr., R. M., Payne, S. W., Recker, E. E. and Reed, R. J. 1979. Structure and properties of synoptic-scale wave disturbances in the intertropical convergence zone of the eastern Atlantic. *J. Atmos. Sci.* **36**, 53–72.

Trenberth, K. E. and Olson, J. G. 1988. Intercomparison of NMC and ECMWF global analyses; 1980–1986. *Technical Note NCAR/TN-301 + STR*, 81 pp. (Available from the National Center for Atmospheric Research, Boulder, CO, 80307–3000.)

Undén, P. 1989. Tropical data assimilation and analysis of divergence. *Mon. Wea. Rev.* **117**, 2495–2517.

Williamson, D. L., Kiehl, J. T., Ramanathan, V., Dickinson, R. E. and Hack, J. J. 1987. Description of the NCAR Community Climate Model (CCM1). *Technical Note NCAR/TN-285 + STR*, 112 pp. (Available from the National Center for Atmospheric Research, Boulder, CO, 80307–3000.)